NASA Technical Memorandum 81422

DYNAMIC MODULUS AND DAMPING OF BORON, SILICON CARBIDE, AND ALUMINA FIBERS

J. A. DiCarlo
Lewis Research Center
Cleveland, Ohio 44135

and

W. Williams
Lincoln University
Lincoln University, Pennsylvania 19352

Presented at the
Fourth Annual Conference on Composites and Advanced Materials
sponsored by the American Ceramic Society
Cocoa Beach, Florida, January 20-24, 1980

DYNAMIC MODULUS AND DAMPING OF BORON, SILICON CARBIDE, AND ALUMINA FIBERS

by

J. A. DiCarlo
Lewis Research Center
Cleveland, Ohio 44135

and

W. Williams
Lincoln University
Lincoln University,
Pennsylvania 19352

E-345

ABSTRACT

The dynamic modulus and damping capacity for boron, silicon carbide, and silicon carbide-coated boron fibers were measured from -190° to 800° C. The single fiber vibration test also allowed measurement of transverse thermal conductivity for the silicon carbide fibers. Temperature-dependent damping capacity data for alumina fibers were calculated from axial damping results for alumina-aluminum composites. The dynamic fiber data indicate essentially elastic behavior for both the silicon carbide and alumina fibers. In contrast, the boron-based fibers are strongly anelastic, displaying frequency-dependent moduli and very high microstructural damping. The single fiber damping results were compared with composite damping data in order to investigate the practical and basic effects of employing the four fiber types as reinforcement for aluminum and titanium matrices.

INTRODUCTION

Measurement of the dynamic mechanical properties of fibers employed for reinforcement of structural composite materials can be both practically and fundamentally useful. On the practical side, since fibers are the primary source of composite stiffness, data for such fiber properties as dynamic

modulus and damping are required by design engineers in order to understand and predict the dynamic response of composite materials that are subject to impact and vibratory loading (1). On the fundamental side, damping measurements can be a very sensitive tool for understanding and monitoring time-dependent deformation mechanisms within a material's microstructure (2). Thus, fiber and composite damping data can be used not only for structural analysis but also for detecting important microstructural changes caused by environmental conditions encountered during composite fabrication and use.

It was with these considerations in mind that the present study was initiated to measure the dynamic modulus and damping capacity of commercially available fibers during various stages before and after composite fabrication. Particular concern centered on the adverse thermal conditions often encountered when the fibers are employed for structural reinforcement of metal matrix composites. For this reason the stages of primary interest were the as-produced fiber, the fiber coated with a protective diffusion barrier, the fiber after composite fabrication, and the fiber after composite use at high temperature. In this paper we report low-strain dynamic property data for boron, silicon-carbide, alumina, and silicon carbide-coated boron fibers. Principal experimental variables were temperatures from -190° to 800° C, stress frequency from 20 to 15000 Hz, and strain amplitude from 10^{-8} to 10^{-5}. In some cases the damping measurement technique also permitted determination of fiber thermal conductivity as a function of temperature.

An important consideration regarding fiber selection for this study was the fact that in previous work we had obtained accurate damping data for the metal matrix composites reinforced by these same fiber types (3,4). To analyze and understand these composite results in terms of all possible structural sources, accurate damping data were required for the constituent

fibers and matrices. For many composite systems in which the constituents are unaffected by composite fabrication conditions, one can assume that the in-situ fiber and matrix damping properties are identical to those measured for the individual constituents in monolithic form. This assumption, however, may not be valid for metal matrix composites for two reasons. First, damping of the metal matrix is very structure-sensitive and thus may be strongly affected by the composite fabrication and the in-situ composite environment. Second, adequate interfacial bonding in metal matrix composites usually required fabrication temperatures high enough to induce significant fiber-matrix reactions. Considering the large surface to volume ratio of the fiber, interfacial reactions could produce measurable effects in the in-situ fiber damping. Therefore, one of the prime objectives of this work was to compare the single fiber results with the metal matrix composite data in order to determine whether any important changes can be detected in constituent damping properties. In addition, if these changes can then be correlated with changes in other microstructure related composite properties, such as, transverse or axial tensile strength, there exists the possibility of utilizing composite damping for nondestructive evaluation (NDE) of metal matrix composites. This NDE capability has already been demonstrated for the axial tensile strength of 6061 aluminum alloy matrices reinforced by boron fibers (4).

An additional consideration concerning fiber selection was based on the observation that aluminum matrix composites reinforced by boron fibers displayed significantly higher damping at all temperatures than titanium and aluminum matrix composites reinforced by silicon carbide and alumina fibers (4). This result suggests that the damping of these latter fibers is much less than that of the boron fiber. The quantitative evaluation of this important damping difference was thus another goal of the present work.

EXPERIMENTAL

Apparatus and Measurement

A simple flexural test was used for measuring the dynamic modulus and damping capacity of single fibers from -190° to over 800° C. The basic test technique consisted of the forced flexural vibration of cantilevered fibers in a high vacuum cryostat-furnace. A schematic diagram of the test setup and associated electronics is shown in Fig. 1.

Fibers with cantilevered lengths from 1 to 4 cm were clamped between two stainless steel plates. The clamp plates contained indentation grooves for accepting various diameter fibers. Each specimen was driven electrostatically at one of its flexural resonant frequencies f_n by applying an alternating voltage at $f_n/2$ between the fiber and a nearby drive plate. The fiber-plate separation was set at ~0.1 mm by means of a screw type manipulator attached to the drive plate. Specimen vibration amplitude was controlled by the output voltage from the drive amplifier. Specimen motion was detected by placing the fiber-plate capacitor into the tank circuit of a 100 MHz RF oscillator (5). Fiber vibrations produced an oscillating capacitance which directly modulated the RF oscillator via a half wavelength coaxial cable. A commercial FM tuner was used to detect these modulations and convert them back to an audio signal with frequency f_n and amplitude directly proportional to that of the specimen.

Dynamic modulus was calculated from the resonant frequencies at which maximum specimen amplitude was observed. Absolute values of the moduli at 20° C were determined by vibrating the specimens in air and then applying the equation (2)

$$E_b = 4\pi^2 \left[\frac{\rho \ell^4}{d^2}\right]\left[\frac{f_n^2}{\alpha_n^4}\right] \qquad (1)$$

Here E_b is the flexural dynamic (storage) modulus; α_n and f_n are the frequency constant and measured resonant frequency for tone n, respectively; and ρ, d, and ℓ are the fiber density, diameter, and cantilevered length, respectively. Since electrostatic drive force varies as the square of the drive voltage, f_n was measured as twice the drive voltage frequency required for maximum amplitude. Due to the large aspect ratio of the fibers ($l/d > 50$), the effects of rotatory inertia and shear deformation on α_n were neglected.

All fiber dimensions were measured optically except for boron fiber diameter. In this case the rough "kernel" surface necessitated "effective" diameter calculations from separate density and mass per length measurements (6). Densities for the other fibers were calculated from optical diameters and mass per length data. Slight corrections for air damping and fiber vibrations within the clamp were made in the final moduli calculations (6).

For temperature dependence of the dynamic moduli, it was convenient to determine the normalized modulus ratio R_b defined as $E_b(T)/E_b(20^\circ\ C)$. The parameter R is more accurate than E because it eliminates fiber dimensional errors. Using Eq. (1), one can calculate R_b directly from the resonant frequency $f_n(T)$ and the fiber thermal expansion coefficient α, i.e.,

$$R_b = \left[\frac{f_n(T)}{f_n(20^\circ\ C)}\right]^2 \left[\frac{1}{1 + \lambda(T)}\right] \qquad (2)$$

where

$$\lambda(T) = \int_{20}^{T} \alpha \, dT$$

The damping capacity ψ measures the percentage of stored mechanical energy lost to heat per cycle of specimen vibration. The vibrational energy losses are a consequence of microstructural deformation mechanisms whose

dynamic stress-strain curves are characteristically hysteretic. In this study flexural damping capacity ψ_b was determined by disconnecting the drive signal and allowing the fiber resonant vibrations to freely decay. The time for the decaying signal to pass between two fixed voltage levels was measured either by oscilloscope photograph or by a Q-meter device developed by Simpson (5). If the initial fiber strain amplitudes were kept below 10^{-5}, all decays were observed to be exponential with decay times independent of strain amplitude. Thus in the low strain region ψ_b can be calculated from

$$\psi_b = \Delta W/W = 2\Delta s/s = \frac{2\ \ell n(s_1/s_2)}{f(t_2 - t_1)} \tag{3}$$

where ΔW is the stored energy lost per cycle, Δs is the signal decrement per cycle, and s_1 and s_2 are the detector signal at times t_1 and t_2, respectively.

At strains above 10^{-4}, boron fiber damping increases with strain amplitude (7), giving rise to nonexponential decays. Since this type of behavior complicates the dynamic measurements, it was decided that data for all fibers would be taken below 10^{-5} maximum strain amplitude. Thus the ψ_b results can be considered as minimum or baseline fiber damping. Under vacuum conditions ($<10^{-5}$ torr), air and apparatus energy losses were negligible, contributing less than 0.0002 to the ψ_b values. Absolute errors in ψ_b were estimated at less than ±5%.

An advantage of measuring E_b and ψ_b as a function of temperature is the possibility of detecting and understanding thermal treatment effects on fiber microstructure. To study these effects in a convenient and systematic manner, the following thermal-cycling procedure was employed. After solvent cleaning and mounting of the as-received fiber, the specimen assembly was

placed under vacuum and rapidly cooled to liquid nitrogen temperature. Dynamic properties were then measured at two specimen resonant tones as the assembly was slowly warmed to a certain treatment temperature above 20° C. After remaining at temperature for a given time, the assembly was slowly cooled to room temperature during which dynamic data was also obtained. A subsequent low temperature run was made from -190° to 20° C. Typical warmup and cooldown rates were 3° C per minute with measurements made about every 10° C. Thermal treatment effects were determined by comparing the warmup and cooldown data.

The Flexural Test Method

Although the flexural vibration of fibers is a simple and accurate test method for determining dynamic properties, one cannot assume that the property results are identical to those obtained by subjecting the fibers to longitudinal vibrations along their axes. The primary source for a possible difference in flexural and axial data is a nonuniform distribution of controlling microstructure across the fiber cross section. That is, the radial strain distribution inherent in flexural deformation tends to weigh more strongly the microstructure near the fiber surface. However, by analyzing the distribution of phases within the fiber and understanding their properties, one can mathematically convert flexural into axial data.

For example, for the typical situation of cylindrically symmetric fiber microstructure, it can be shown that the average dynamic modulus and damping capacity values measured in a particular test are given by (9)

$$E = \int_0^{r_1} E(r)\left[\varepsilon(r)\right]^2 r\, dr \Big/ \int_0^{r_1} \varepsilon^2 r\, dr \qquad (4)$$

and

$$\psi = \int_0^{r_1} \psi(r)E(r)[\varepsilon(r)]^2 r\, dr \Big/ \int_0^{r_1} E\varepsilon^2 r\, dr \qquad (5)$$

Here r_1 is the fiber radius and $\varepsilon(r)$ is the strain amplitude for a fiber element at position r. For a flexural or bend (subscript $\underline{b}$) test, ε is directly proportional to r; whereas for an longitudinal or axial (subscript $\underline{a}$) test, ε is independent of r. Thus E_b and ψ_b will equal E_a and ψ_a only when $E(r)$ and $\psi(r)$ are independent of radial position. Obviously this is not the case for most fibers since they contain heterogeneities such as cores and surface diffusion barriers. Nevertheless, by analyzing fiber structure and assigning proper E and ψ values to the different phases, one can combine Eqs. (4) and (5) with measured flexural data and thus arrive at fairly accurate predictions for fiber axial properties.

Besides simplicity, an additional advantage of the flexural test is that in certain situations it can be used to determine transverse thermal conductivity. This is due to the fact that during flexure, internal transverse thermal gradients are generated due to coupling between local stress and temperature. If the vibrational period of the stress is near the relaxation time for thermal diffusion across the specimen thickness, mechanical energy losses arise producing "thermoelastic damping" which is additive to the specimen's microstructural damping. For a fiber specimen of cylindrical cross section, the thermoelastic damping capacity ψ_{TE} at a stress frequency f is given by (2)

$$\psi_{TE} = \psi_{TE}^{max} \left[2\, ff_o/(f^2 + f_o^2)\right] \qquad (6)$$

where

$$\psi_{TE}^{max} = \pi E \alpha^2 T/\rho C \tag{7}$$

and

$$f_o = 2.16\ K/\rho C d^2 \tag{8}$$

Here C, ρ, d, E, α, K, and T are the specific heat, density, diameter, axial Young's modulus, axial thermal expansion coefficient, effective transverse thermal conductivity, and average absolute temperature of the fiber. Eq. (6) indicates that ψ_{TE} is symmetrical around $f = f_o$ and reaches its maximum value ψ_{TE}^{max} at $f = f_o$. Thus if the thermoelastic frequency f_o for a particular fiber falls conveniently within the frequency range of the vibration detection system and if ψ_{TE} is an appreciable fraction of the total ψ_b, one can determine f_o and ψ_{TE}^{max} by damping versus resonant frequency measurements. By measuring f_o at different temperatures, one can then utilize Eq. (8) to determine fiber transverse thermal conductivity as a function of temperature.

Fiber Specimens

All fibers studied in this report were obtained from commercial vendors. They include 142 and 203 μm diameter boron on tungsten, B(W); 103 μm silicon carbide on tungsten, SiC(W); 143 μm silicon carbide on carbon, SiC(C); 145 μm silicon carbide-coated boron on tungsten, (SiC)B(W); and 20 μm alumina, Al_2O_3.

The B(W), SiC(W), and SiC(C) fibers, obtained from Avco Specialty Materials Division, were produced by chemical vapor deposition onto resistively-heated wire substrates. During deposition of the B(W) fibers the original 12.5 μm tungsten substrate was converted to a 17 μm tungsten boride "core" within an amorphous boron "sheath." The substrates for the

SiC fibers reacted little with the deposited sheath material so that the effective core diameters remained at 13 μm for tungsten and 37 μm for carbon. The stoichiometric SiC sheaths were polycrystalline with the β cubic form. The SiC(W) fibers have no surface coating, but a ~1 μm thick graded carbon coating was deposited on the SiC(C) surface to decrease its sensitivity to flaws induced by handling.

The (SiC)B(W) fibers were obtained from Composite Technology Inc. under the "Borsic" tradename. They were included in this study in order to investigate the possible microstructural effects of depositing a 1.5 μm SiC coating onto 142 μm B(W) fibers.

The small diameter Al_2O_3 fibers were obtained from DuPont under the tradename "FP alumina." These fibers which were produced by a proprietary technique are polycrystalline with no core. The absence of a conducting core coupled with their high resistivity made is impossible to electrostatically drive the Al_2O_3 fibers in their as-produced condition. To circumvent this conduction problem a very thin gold coating was added to the fiber surface. Although vibration could then be achieved, the damping of the composite fiber was amplitude dependent, continuously decreasing as strain was reduced down to noise levels ($\sim 10^{-8}$). This effect was probably due to an amplitude-dependent damping for the gold coating which is additive to the Al_2O_3 damping. Thus the lowest damping measured can be considered only as an upper limit data point for alumina fiber damping capacity at room temperature. However, as will be discussed, this point is in good agreement with Al_2O_3 fiber damping calculated from temperature-dependent axial damping data for Al_2O_3/Al composites (4).

RESULTS AND DISCUSSION

Dynamic Modulus

Room Temperature. - The 20° C experimental results for fiber density ρ and dynamic flexural modulus E_b are listed in Table 1. The ρ data represent the average of three different specimens, whereas the E_b data represent the average taken from one specimen vibrated at four tones at each of four different cantilevered lengths. Standard deviations are indicated in parenthesis. Also included in Table 1 are calculated values for the sheath density ρ_s and the fiber dynamic axial modulus E_a. These calculations were made using the experimental data plus the core and coating properties listed in Table 2. The last column of Table 1 lists room temperature quasistatic axial moduli as measured by other investigators.

The primary error source in the ρ and E_b data for the (SiC)B and SiC fibers was variation in fiber diameter along the specimen length. Typically, optical diameter measurements accurate to ± 0.1 μm were made every centimeter along an 8 cm long fiber specimen. Since ρ and E_b depend on the second and fourth power of fiber diameter, respectively, a small diameter variation can produce a large effect in these parameters. For the B(W) fibers, the diameter variation effect on ρ was eliminated by use of a liquid density gradient column accurate to ± 0.001 gm/cm^3. By measuring ρ directly and combining the result with a sensitive mass measurements for the total fiber length, we were also able to obtain low variation "effective" diameter data for use in the E_b calculations. In contrast, the Al_2O_3 fibers had such small and variable diameters that no accurate diameter, density, or modulus measurements could be made. Thus the alumina values listed in Table 1 were obtained from Dupont (11) and are only included for comparison purposes.

The E_b moduli of Table 1 were measured at frequencies between 10^2 and 10^4 Hz. Within the accuracy of the E_b measurement, no dependence on frequency could be observed in this range. That the E_b results should be frequency independent was supported by simultaneous measurements of very low fiber damping. That is, low damping is indicative of closed dynamic hysteresis loops and thus of dynamic strains in phase with dynamic stresses. Changing the stress application rate by changing the frequency between 10^2 and 10^4 Hz should therefore have negligible effect on the instantaneous or dynamic moduli (8). That is not to say, however, that effects would not be observed by operating at significantly faster or slower stress rates, as for example, in a slow bend or tensile test. Indeed, the damping versus temperature results to be discussed will indicate that frequency variation over several orders of magnitude will negligibly affect the 20° C dynamic moduli of the SiC and Al_2O_3 fibers but can have measurable effects on the moduli of the boron-based fibers. For this reason one should consider only the Table 1 SiC and Al_2O_3 moduli results to be truly frequency independent.

To analyse the E_b data in terms of their structural sources and then convert this information into dynamic axial moduli E_a, we employed Eq. (4) for the theoretical modulus of a multiphase fiber. The properties assigned the core and coating phases are listed in Table 2. Regarding the sources for flexural moduli, one finds that for the fiber diameters of this study, the tungsten and carbon cores play essentially no role. Thus the E_b results of Table 1 represent the flexural moduli of the sheath material plus any surface coating. From the boron fiber results it is apparent then that the 1.5 μm SiC coating measurably increases the E_b for B(W) fibers. On the other hand, the low modulus carbon coating on the SiC(C) fiber appears to decrease the SiC sheath modulus. The existence of this low density carbon coating is also evident in the ρ_s result for SiC(C).

The dynamic axial moduli E_a calculated from the E_b data are also listed in Table 1. These results indicate that E_a and E_b are essentially equal as long as cores and coatings have low volume fractions and moduli similar to that of the sheath. However, the SiC(C) data shows that the 37 μm carbon core with large volume fraction and low modulus can produce an E_a smaller than E_b. Comparing the dynamic results with literature data for quasistatic E_a, one finds very good agreement for both types of SiC fibers. This agreement supports the fact that at low temperature the moduli of chemically varpor-deposited SiC fibers are frequency independent. For the B(W) fibers, the apparent agreement between the quasistatic E_a and the dynamic E_b is misleading in that due to anelasticity, boron moduli should be higher when measured dynamically. DiCarlo has suggested that a low flexural modulus may be a direct result of a lower than average density for the outer layers of the boron sheath (6). In this case, the higher (SiC)B(W) moduli might then be explained in part by a B(W) sheath densification during deposition of the SiC coating. Finally, although no E_b measurements could be made for the Al_2O_3 fibers, the very low damping of this fiber plus the absence of a coating or core suggest that its dynamic E_b and E_a are truly frequency independent and thus equal to the quasistatic modulus of 362 ± 17 GN/m^2.

Temperature Dependence. - To determine the normalized modulus ratio $R_b = E_b(T)/E_b(20^\circ C)$, fiber resonant frequencies were measured approximately every 10° C from -190° to over 800° C. The frequency data was then inserted into Eq. (2) to yield the R_b results of Fig. 2. Thermal expansion coefficients required for the λ calculations were obtained from Ref. 6 for boron fibers and from Ref. 13 for bulk silicon carbide. Actual data points are not shown in Fig. 2 because they were taken about 10° C apart with an average error in R of less than ± 0.003.

The boron fiber R_b data were found to be measurably frequency and temperature dependent at temperatures just above 100° C. This effect is illustrated in Fig. 2 by first and second tone data for a single length B(W) fiber. DiCarlo has attributed this behavior to time-dependent anelastic creep mechanisms within the CVD boron (6). The possible structural defects responsible for these mechanisms will be discussed with the damping results. Suffice to say here, that whenever the applied stress frequency f begins to become comparable to the thermally-activated motion rate ν for the defects, measurable dynamic creep effects occur which manifest themselves in a damping increase and a dynamic modulus decrease. By analysis of boron creep data, DeCarlo has been able to predict modulus dependence on frequency and temperature. His predicted R_b curve when f is so much larger than ν that no creep effects can occur is shown by the dashed line of Fig. 2. Comparing this curve with B(W) results, one finds that creep effects are unobservable for frequencies above 10^2 Hz and temperatures below 100° C. Outside this frequency-temperature region, however, dynamic creep can produce significant effects on boron fiber dynamic modulus.

In contrast to the boron results, the R_b curves for both the SiC(W) and SiC(C) fibers were observed to be identical and frequency independent up to at least 600° C. These findings indicate the absence of any significant time-temperature dependent creep mechanisms with the chemically vapor deposited SiC sheath. Thus the single SiC curve of Fig. 2 represents baseline dynamic and quasistatic modulus behavior for both types of SiC fibers.

To convert the R_b results into practical axial moduli data we have assumed that the relative contributions of the cores and coatings change negligibly with temperature so that $E_a(T) = R_b(T)E_a(20^\circ\ C)$. The E_a

results for the various fibers are shown in Fig. 3. Also included is the Dupont data for the quasistatic axial modulus of the Al_2O_3 fiber. As the damping versus temperature results for this fiber will show, time-dependent deformation mechanisms are essentially absent so that its dynamic modulus is frequency independent and thus equal to its quasi-static modulus. Comparing the Fig. 3 data, one finds that although all fibers have equivalent dynamic moduli near room temperature the boron fiber E_a drops off much more rapidly with temperature than that for SiC or Al_2O_3. Also, although the SiC and Al_2O_3 moduli are frequency independent, the E_a for boron has a strong dependence on frequency stress rate. This effect becomes especially dramatic in slow rate tensile test as evidenced by the circle data points (14) included in Fig. 3. Thus design situations which require elevated temperature use of fiber reinforcement, one must be especially cognizant of the frequency dependence of boron fiber stiffness.

Damping

Because many composite applications entail dynamic loading at elevated temperature, measurement of the temperature-dependence of fiber damping has a clear practical significance. Such data is also important fundamentally in that the damping measurement is a sensitive tool for monitoring time-dependent creep mechanisms associated with defects within the fiber microstructure. The physical basis for this sensitivity is the fact that various defects such as impurities, dislocations, and grain boundaries move locally within the microstructure with a thermally-activated jump frequency ν. That is,

$$\nu_i = \nu_i^o \exp(-Q_i/kT) \tag{9}$$

where k is Boltzmann's constant, T is absolute temperature, and ν_i^o and Q_i are the jump frequency constant and activation energy characteristic of

a type i defect. When the applied stress frequency is considerably less or greater than ν_i, creep strains associated with i defect motion are out of phase with the stress, resulting in zero damping contribution from these defects. However, when $f = \nu_i$, creep effects are maximized, resulting in a damping peak with a height proportional to the defect i concentration. Thus measurements of fiber damping versus temperature will generally yield a "spectrum" of damping peaks centered at temperatures T_i where the defect jump frequency ν_i become equal to the applied frequency. By measuring the damping spectrum at another frequency, one observes a shift in T_i which can then be used with Eq. (9) to determine ν_i^o and Q_i and thus to identify the various defect types within the fiber.

In the sections that follow, damping capacity curves for as-produced and heat-treated fibers will be presented and discussed first. Again for clarity purposes actual data points will not be shown since they were taken about every 10^o C and fell to within $\pm 3\%$ of the best fit curves. The single fiber results will then be compared with low temperature damping data for metal matrix composites in order to investigate the sources of composite damping and also possible fiber and matrix property changes caused by composite fabrication and thermal treatment.

Boron Fibers. - Presentation of the damping spectra for the boron-based fibers is complicated by the fact that between -190^o and 800^o C, damping capacity changed by two orders of magnitude. Therefore, in order not to compromise the sensitivity of the ψ measurement, the boron data are shown in three temperature regions: low, elevated, and high in Figs. 4(a), (b), and (c), respectively. Within these figures curve a refers to warmup data for as-received fibers, whereas curve b refers to both warmup and cooldown data after fiber heat treatment above 400^o C. The solid curves were measured

at the first (300 Hz) and second (1800 Hz) tones of a single length B(W) fiber. The dashed curve is second tone (1000 Hz) data for a (SiC)B(W) fiber. Except for slight diameter-dependent effects caused by thermoelastic damping (to be discussed), the Fig. 4 results were reproducible from specimen to specimen to within ±5%. Also the B(W) data were unaffected by etching as-received 203 μm fibers to ~50% of their original diameters. This observation indicates that the B(W) damping results were independent of conditions on or within the surface layers of the as-produced fibers.

The low temperature damping data for as-received boron-based fibers were found to be exactly reproducible as long as heat treatment temperatures were kept below 150° C. A typical damping spectrum for B(W) fibers is shown by curve a (1800 Hz) of Fig. 4(a). This curve displayed two very small peaks labelled A and B on top of a slightly rising background. Heating the as-received fibers above 150° C resulted in some unknown annealing effects within the boron sheath as evidenced by a drop in background damping. This can be observed by comparing the 300 Hz a and b curves of Fig. 4(b). Near 400° C the annealing effects were complete, yielding the stable b curves which were reproducible during subsequent warmups to 800° C.

The high temperature results of Fig. 4(c) show that the background damping is itself the low temperature tail of a significantly large, broad, and frequency-dependent damping peak labelled Peak I. The practical importance of Peak I becomes obvious when one realizes that even at dynamic strains below 10^{-5}, boron fibers can lose from 1 to 24% of their mechanical energy during each cycle of vibration. Indeed, by virtue of their correlation in temperature and frequency, it follows that the creep mechanisms

responsible for Peak I also produced the large dynamic modulus decreases seen in Figs. 2 and 3. Equations for predicting these effects at other frequencies and higher vibrational strains have been developed (6) but will not be discussed here.

To determine whether the Fig. 4 results apply also for axial vibrations, it is convenient to separate the various phase contributions to fiber flexural damping ψ_b and axial damping ψ_a as follows:

$$\psi_b = \beta_s\psi_s + \beta_c\psi_c + \beta_x\psi_x \tag{10}$$

and

$$\psi_a = \gamma_s\psi_s + \gamma_c\psi_c + \gamma_x\psi_x \tag{11}$$

where the subscripts s, c, and x refer to the sheath, core, and coating phases, respectively. Equation (5) and the phase properties of Tables 1 and 2 were used to calculate the Table 3 values for the β and γ coefficients of the various multiphase fibers. At temperatures below 400° C, damping capacity values for tungsten-boride cores removed from B(W) fibers were measured to be less than 0.4%. This result plus Table 3 indicate that for B(W) fibers, $\psi_b = \psi_a = \psi_s$ = boron sheath damping to within an error of less than 2%. Regarding the (SiC)B(W) fibers, one can assumed (from the SiC fiber results to follow) that $\psi_x < 0.2\%$ for the SiC coating, so that $\psi_b = 0.98\ \psi_a$. Thus, to within the accuracy of the ψ_b measurement ($\pm 5\%$), the Fig. 4 results can indeed be considered as boron fiber axial damping data.

Identification of the microstructural sources for the peaks in the boron fiber damping spectra is best accomplished first by a determination of peak height and relaxation rate parameters and then by experimental studies

to understand how these parameters are affected by controlled environmental conditions. DiCarlo has performed such a study for Peaks A, B, and I in the B(W) fibers (15). Although no conclusions were made concerning Peaks A and B, it appears that Peak I is the result of the localized motion of substructural units which like grains comprise the whole volume of the boron sheath. These units were tentatively identified as B_{12} icosahedra which are clusters of 12 boron atoms. In the present study a new element has been added in that damping results now exist for a boron sheath coated with a SiC coating. From a basic point of view it is of interest to consider just what new microstructural information can be extracted by close examination of these results.

First, because both boron-based fibers were produced at temperatures well above 1000° C, one might not expect to observe the background annealing effect when the fibers are reheated to only 150° C. The fact that annealing does occur in both fiber types suggests that a necessary condition for its existence is the rapid quench experienced by the boron sheath when the fibers leave the CVD reactor. Perhaps on the microstructural level, the quench freezes some B_{12} icosahedra into localized high damping states. When allowed to move again at temperatures near 200° C, these icosahedra move into positions that contribute lower damping. Another observation is that Eq. (10) and the Table 3 parameters predict that ψ_b for (SiC)B(W) should be about 98% the ψ_b for B(W). Comparing the Fig. 4 results (b curves) for the two fiber types and neglecting slight frequency effects, one indeed finds a lower damping for (SiC)B(W), but measurably less than predicted. This effect could be due to microstructural differences in the boron sheaths since the two fiber types were produced by two different manufacturers. Another possible explanation is that besides reducing ψ_b by virtue of its volume, the SiC coating somehow also reduces the boron sheath ψ_s by

affecting those defect mechanisms responsible for the low temperature side of peak I. This second interpretation seems more likely since similar damping reduction effects have been observed whenever B(W) fibers are heated in oxygen (3) or in aluminum matrix composites (to be discussed). Thus from a practical point of view, it would appear that the addition of surface phases may be a method of reducing boron fiber damping and also increasing its dynamic modulus, whereas a rapid quench from high temperature may be a method of achieving just the opposite.

One final point is that the existence of Peaks A and B in the B(W) fibers and their apparent absence in the (SiC)B(W) fibers suggest that the peaks' sources may be impurities introduced into the boron sheath by the production techniques employed by the B(W) manufacturer. If indeed future work on specially-doped fibers proves this to be the case, the damping measurement could then become useful for fiber impurity analysis.

Silicon-Carbide Fibers. - In contrast to the boron fiber data, the damping versus temperature spectra for the SiC fibers were relatively structureless and low in value. The flexural damping capacity results measured for the 1st, 4th, and 9th tone of a single length 103 μm SiC(W) fiber are shown in Fig. 5. These results were unaffected by thermal treatments up to 800° C. As indicated by Fig. 5, the major variable for ψ_b was the applied stress frequency. Typically as frequency increased, fiber damping increased and then decreased. As will be discussed, this peaking of damping with frequency is evidence that a major contribution to ψ_b was the thermoelastic damping ψ_{TE} caused by transverse thermal currents during fiber flexure. Although the existence of such an effect could be used to determine fiber thermal conductivity, its presence served to complicate measurement of ψ_b^*, the flexural damping produced only by microstructural mechanisms within the SiC

fibers. It therefore became necessary to measure ψ_{TE} and then eliminate it from the ψ_b data.

Typical data required for determination of ψ_{TE} are shown in Fig. 6. In this case damping measurements were made on a single length 103 μm SiC(W) fiber vibrated at its nine lowest tones at 26° C. The ψ_b results show a symmetric damping peak with shape and height characteristics in good agreement with the thermoelastic predictions of Eqs. (6) and (7). Thus knowledge of the frequency f_o at the peak maximum can be used not only to determine ψ_{TE} at any applied frequency but also to calculate fiber thermal conductivity (Eq. (8)). By obtaining data such as that shown in Fig. 6 at various temperatures, it was thus possible to convert ψ_b data into ψ_b^* data for any tone of the SiC fibers. The ψ_b^* results for the data of Fig. 5 are shown in Fig. 7. These results are essentially equivalent to ψ_b^* data obtained from damping measurements on SiC(C) fibers (dashed curve).

Examining the microstructural damping results of Fig. 7, one observes negligible dependence on frequency or temperature except near -200° C and 800° C. From a basic point of view, this result indicates the relative absence of creep-related defect mechanisms in the chemically vapor-deposited SiC sheath. The relaxation parameters or the defects associated with the -200° C and 800° C peaks have not been determined. Both peaks, however, are somewhat larger in the SiC(C) fibers, perhaps suggesting some role of the carbon-rich surface layer. To understand the sources for the 800° C peak, higher temperatures or lower frequencies are clearly required. The temperature region of its appearance suggests grain boundary sliding as its possible source.

Whether the ψ_b^* results of Fig. 7 are equivalent to ψ_a for an axially vibrated SiC fiber is difficult to determine theoretically since tungsten and

carbon core damping are not known. Experimentally, however, the very low values and the equivalence of the ψ_b^* for SiC(W) and SiC(C) indicate the cores contribute negligibly to the flexural results. Also the metal matrix composite data to be discussed shortly are best explained by assuming $\psi_a = \psi_b^*$. Thus one might conclude that in general core contributions are zero and the Fig. 7 data are accurate representations of ψ_a for the SiC fibers. It follows then that at all temperatures the boron-based fibers display a significantly larger ψ_a than the silicon-carbide fibers. The practical significance of this damping difference will become apparent in following section on composite damping.

Composite Damping

To determine whether the damping results for single fibers can be used to directly predict damping for metal matrix composites, we have employed the low-strain axial damping data measured by DiCarlo and Maisel (4) for the following unidirectional composites: 6061 and 1100 aluminum alloys reinforced by 203 μm B(W) and 145 μm (SiC)B(W) fibers; titanium-6Al-4V alloy titanium reinforced by 142 μm SiC(C) fibers; and aluminum-2Li alloy reinforced by 20 μm Al_2O_3 fibers. In their studies DiCarlo and Maisel investigated the predictability of composite dynamic moduli in terms of constituent moduli. However, due to a low lack of accurate fiber and matrix damping data, they were unable to examine in detail the structural sources responsible for composite damping. With the single fiber data of this study, we are now in a position to investigate these sources and by so doing shed some light on possible effects of composite environment on fiber and matrix damping.

For unidirectional composites vibrated axially along their fiber axes, dynamic theory (16) similar to Eq. (5) predicts an axial damping capacity ψ_{11} given by

$$\psi_{11} = \gamma_{11}\psi_F + (1 - \gamma_{11})\psi_M \qquad (12)$$

where $\gamma_{11} = v_F(E_F/E_{11})$. Here v_F is fiber volume fraction, E_{11} is the axial dynamic modulus of the composite, and the subscripts F and M refer to the fiber and metal matrix phase, respectively. For the purpose of examining the ψ_{11} data of DiCarlo and Maisel, we have assumed that ψ_F, the axial damping of the in-situ fibers, is equal to ψ_b, the flexural damping as measured on single fibers after heat treatment at composite fabrication temperatures. Regarding matrix damping, one cannot assume that ψ_M is the same as that measured on a monolithic specimen of the same metal alloy. This is due to the fact that in contrast to ceramic type materials, metals generally exhibit a very structure sensitive damping which is controlled by dislocation motion at low temperature and grain boundary motion at high temperature. Since these defects and their mobilities can be altered significantly during composite fabrication and cooldown and also during specimen preparation procedures, the approach taken here was to consider only those situations where the matrix contribution to composite damping $(1 - \gamma_{11})\psi_M$ can be assumed to be zero. As will be shown, one such situation appears to exist in the low temperature damping results for metal matrix composites which were heat treated at recrystallization temperatures for the matrix. Apparently the heat treatment reduces dislocation density and mobility, thereby decreasing low temperature ψ_M to very small values. An additional factor that reduces matrix contributions is the high fiber to matrix modulus ratio which for 50% fiber volume fraction yields γ_{11} values of about 80%.

Low temperature axial damping ψ_{11} data for boron/aluminum composites vibrating near 2000 Hz are shown in Fig. 8. The a curve was measured after composite panel fabrication, diamond cutting, and specimen mounting.

It represents to within ±10% the results from 203 μm B/6061 Al, 203 μm B/1100 Al, 142 μm B/6061 Al, and 145 μm (SiC)B/6061 Al specimens. Fiber volume fraction for all composites was 50 ± 2%. After in-situ vacuum heat treatments up to a maximum of 400° C, the composite ψ_{11} were observed to diminish, reaching the minimum damping shown by curve b for B/Al and by curve c for (SiC)B/Al. Since composite fabrication temperatures were 460° C and above, the decrease in ψ_{11} was due to a decrease in ψ_M caused by annealing effects on matrix dislocations created during specimen preparation.

To understand fiber contributions to the B/Al data, one can examine the term $\gamma_{11}\psi_F$ in Eq. (12). Taking $\gamma_{11} = 0.84$ and assuming the ψ_F are given by the post heat-treatment curves of Fig. 4, one then obtains the fiber contributions shown by the Fig. 8 dashed curves. As can be observed, good agreement exists between the (SiC)B fiber and heat-treated composite curves. This implies that composite annealing effectively reduces ψ_M effectively to zero, leaving the fibers as the only source of B/Al damping at low temperature. It also indicates that no detectable changes occurred in (SiC)B damping during composite fabrication. On the other hand, the fact the B(W) fiber curve is greater than the heat-treated B/Al curve suggests that the damping of in-situ B(W) fibers is measurably less than that of the as-produced and heat-treated fiber. Thus, unlike (SiC)B(W), the damping of uncoated B(W) fibers appears to be affected by composite fabrication conditions in general and most probably by fiber-matrix reactions in particular. The close agreement between composite curves b and c suggests that the fiber-matrix interfacial reaction necessary for good bonding produces a similar change in B(W) damping as the addition of the SiC diffusion barrier coating. One possible practical implication of these surface reaction-damping

relationships is that the damping of annealed B/Al composites might be used to monitor the degree of fiber-matrix bonding.

Axial damping data for a Ti-6Al-4V composite reinforced by 142 μm SiC(C) fibers are shown in Fig. 9. Curve a is first warmup data, whereas curve b is the stable data after heat treatment at 590° C. As in the case of B/Al, effects of matrix annealing are seen as a drop in composite damping. The fiber contribution $\gamma_{11}\psi_F$ to composite damping is shown by the dashed line. In this case, v_f = 44%, γ_{11} = 75%, and ψ_F is the ψ_b^* for SiC(C) in Fig. 7. The good agreement between the fiber and heat-treated composite curves is a clear indication that after composite annealing, negligible damping is available from the matrix up to at least 300° C. Above this temperature, large damping effects due to grain-boundary sliding within the titanium matrix become evident. The agreement also implies that as-produced SiC fiber results of Fig. 7 are a good representation of in-situ fiber damping. On the basic side, this property stability allows one to remove SiC fiber contributions from composite damping and thus study directly the effects of composite environment on matrix damping and microstructure. An interesting point in this regard is that after composite annealing, matrix damping does not appear to increase during cooldown even though the matrix should be experiencing cold-working by means of fiber related residual stresses.

The above analyses for B/Al and SiC/Ti damping have shown that the axial damping for a composite annealed at matrix recrystallization temperatures is essentially the in-situ fiber axial damping reduced by a factor γ_{11}. This result implies that the in-situ damping of Al_2O_3 fibers can be determined directly from the ψ_{11} data for alumina/aluminum composites shown in Fig. 10. Curve a is first warmup results and curve b the results after heat treatment at 560° C. Considering ψ_M to be zero after heat treatment, one can

divide the curve b by $\gamma_{11} = 0.84$ to obtain the dashed curve for in-situ Al_2O_3 fiber damping. The dashed curve thus represents the upper limit damping to be expected from the alumina fibers. The 20° C data point measured on an as-received fiber suggests that the calculated fiber curve is indeed an accurate representation of fiber damping both for as-received and in-situ Al_2O_3 fibers.

As a final point concerning the effects of composite conditions on fiber damping, DiCarlo and Maisel heat treated B/6061 Al composites at temperatures above 460° C in order to produce appreciable fiber-matrix reaction. Such treatment is known to cause serious degradation in fiber and composite tensile strength (17). Measuring composite damping after thermal treatment, they observed near 250° C the growth of a damping peak whose height could be correlated with losses in composite strength. The source of the extra damping appears to be in ψ_M due possibly to boron atom diffusion into the matrix. Using the data on heavily reacted composites, attempts were made in the present study to determine whether microstructural related changes could also be detected in ψ_F. Low temperature axial composite data indicate that after the initial bonding reaction during composite fabrication, no further decreases could be observed in fiber damping, even though reactions were occurring which cause significant strength losses. Thus at least for B/Al, any NDE capability of the damping measurement for monitoring tensile strength must rely on reaction-related changes in high temperature (250° C) matrix damping. Damping measurements on SiC/Ti and Al_2O_3/Al composites after heat treatment at excess temperatures have yet to be made.

Thermal Conductivity

For the SiC(W) and SiC(C) fibers, damping data such as those shown in Fig. 6 were employed to determine the thermoelastic parameter f_o as a

function of temperature. Accurate f_o measurements were possible because these fibers satisfied two experimental conditions. First, specimen properties and diameters were such that the peak of the thermoclastic damping fell conveniently within the frequency range of the audio drive and detection systems. Second, the shape and magnitude of ψ_{TE} could be clearly distinguised from the microstructural damping ψ_b^*. For the B(W) and (SiC)B(W) fibers of this study, the second condition was not realized due to a large and frequency dependent ψ_b^*. Even at room temperature and below where ψ_b^* for these fibers is small and fairly frequency-independent, it is estimated that $\psi_{TE} < 0.1\ \psi_b^*$ for frequencies near 1000 Hz.

With knowledge of f_o it was then possible to employ Eq. (8) to calculate the transverse thermal conductivity K for the SiC(W) and SiC(C) fibers. The results shown in Fig. 11 are based on the bulk SiC specific heat data of Ref. 13. For comparison purposes, thermal conductivity data for bulk β-silicon carbide (18) are also included in this figure. These data suggest that the larger low-conductivity carbon core reduces fiber transverse conductivity, whereas the smaller high-conductivity tungsten core enhances conductivity. However, because SiC thermal conductivity is strongly influenced by impurities (19), it may be sheath purity rather than core type that is the prime factor controlling the Fig. 11 results.

SUMMARY AND CONCLUSIONS

A single fiber flexural vibration test was employed to measure the dynamic modulus and damping capacity of boron, silicon carbide, and silicon carbide-coated boron fibers from -190^{o} to 800^{o} C. The test was also used to determine the transverse thermal conductivity for the silicon carbide fibers. Maximum strain amplitudes were maintained below 10^{-5} and applied stress frequencies between 20 and 15000 Hz. Because the single fiber test could not be employed for alumina fibers, damping data for alumina/aluminum composites

were used to calculate Al_2O_3 fiber damping capacity from -190° to over 100° C. The dynamic property results indicate essentially elastic deformation behavior for both the SiC and Al_2O_3 fibers. On the other hand, the boron-based fibers are strongly anelastic near room temperature and above. This anelasticity is manifested by frequency-dependent dynamic moduli and very high microstructural damping.

From a practical point of view, previously measured composite data indicate that the single fiber dynamic properties are insignificantly affected by the adverse environmental conditions encountered during the fabrication and thermal treatment of metal matrix composites. Thus the nonelastic or time-dependent deformation of composites will be matrix controlled for SiC and Al_2O_3 reinforcement and both matrix and fiber controlled for boron reinforcement. For dynamic response this means that boron fibers will contribute to the frequency-dependence of composite moduli at elevated temperature. But it also means that the damping for these composites will be considerably larger than the damping for composites reinforced by SiC or Al_2O_3 fibers. In many situations a large fiber damping contribution may be a desirable property. One good example is the metal matrix composite after thermal treatment (annealed condition) since for this material the fibers are apparently the only source of composite damping.

On the microstructural level it appears that boron fiber damping can be increased by rapid quenching from deposition temperatures and possibly decreased by the addition of a SiC coating. Low temperature composite damping data indicate that the damping of uncoated boron fibers is also reduced during B/6061 Al composite fabrication. Subjecting these composites to temperatures in excess of the fabrication temperature produced no additional change in fiber damping but measurably increased matrix damping near 250° C (4). These observations suggest that for B/6061 Al composites, damping measurements near

room temperature can be employed to nondestructively evaluate the onset of fiber-matrix bonding and damping measurements near 250° C to nondestructively evaluate tensile strength degradation effects associated with excess fiber-matrix reaction. Finally, due to the very low and stable damping of the SiC and Al_2O_3 fibers, one can mathematically remove their contributions from composite damping measurements and thus use the results to perform basic studies on the effects of composite environment on matrix damping and microstructure.

NOMENCLATURE

C	specific heat
d	diameter
E	Young's modulus
f	frequency
f_o	thermoelastic frequency
K	thermal conductivity
ℓ	length
Q	activation energy
r	radial position from fiber axis
s	signal voltage
T	temperature (Kelvin)
t	time (seconds)
v	volume fraction
W	mechanical energy
α	thermal expansion coefficient
α_n	frequency constant for tone n
β	flexural damping coefficient
γ	axial damping coefficient
ε	strain
λ	thermal strain
ν	defect jump rate
ρ	density
ψ	damping capacity

Subscripts:

a	axial (longitudinal)
b	bend (flexural)
c	core

F fiber

i characteristic of i^{th} defect

M matrix

n tone number

S sheath

X surface phase

TE thermoelastic

11 along fiber axes in unidirectional composite

REFERENCES

1. B. J. Lazan, Damping of Materials and Members in Structural Mechanics, Pergamon Press, New York, 1968.

2. A. S. Nowick and B. S. Berry, Anelastic Relaxation in Crystalline Solids, Academic Press, New York, 1972.

3. J. A. DiCarlo and J. E. Maisel, "Measurement of the Time-Temperature Dependent Dynamic Mechanical Properties of Boron/Aluminum Composites," Fifth Conference on Composite Materials: Testing and Design, 5th, ASTM-STP-674, American Society for Testing Materials, Philadelphia, 1979, pp. 201-227.

4. J. A. DiCarlo and J. E. Maisel, "High Temperature Dynamic Modulus and Damping of Aluminum and Titanium Matrix Composites," NASA TM-79080, 1979.

5. H. M. Simpson and A. Sosin, "Automatic Internal Friction and Modulus Measurement Apparatus Utilizing a Phase-Locked Loop," Rev. Sci. Instrum., 48 (11) 1392-1396 (1977).

6. J. A. DiCarlo, pp. 520-538 "Mechanical and Physical Properties of Modern Boron Fibers," Second International Conference on Composite Materials, Edited by B. R. Noton, The Metallurgical Society of AIME, New York, 1978.

7. T. E. Firle, "Amplitude Dependence of Internal Friction and Shear Modulus of Boron Fibers," J. Appl. Phys., 39, 2839-2845 (1968).

8. A. S. Nowick, pp. 1-70 "Internal Friction in Metals," Progress in Metal Physics, Edited by B. Chalmers, Interscience Publishers, New York, 1953.

9. R. H. Ericksen, "Room Temperature Creep and Failure of Borsic Filaments," Fibre Sci. Technol., 7 (3) 173-183 (1974).

10. R. L. Crane, "An Investigation of the Mechanical Properties of Silicon Carbide and Sapphire Filaments," Report No. AFML-TR-72-180, Sep. 1972.

11. A. R. Champion, W. H. Krueger, H. S. Hartmann, and A. K. Dhingra, pp. 883-904 "Fiber FP Reinforced Metal Matrix Composites," Second International Conference on Composite Materials, Edited by B. R. Noton, the Metallurgical Society of AIME, New York, 1978.

12. J. A. McKee and L. A. Joo, pp. 536-551 "New Carbon Monofilament Substrate for Chemical Vapor Deposition," Proceedings of the Third International Conference on Chemical Vapor Deposition, Edited by F. A. Glaski, American Nuclear Society, Hinsdale, IL, 1972.

13. Y. S. Touloukian, ed., Thermophysical Properties of High Temperature Solid Materials, Vol. 5, Macmillan Co., New York, 1967.

14. J. L. Cook and T. T. Sakurai, pp. H1-H11 "Stress-Rupture and Tensile Test Techniques for Single Boron Filaments at Room and Elevated Temperatures," Advanced Fibrous Reinforced Composites, Vol. 10, Society of Aerospace Material and Process Engineers, Azusa, CA, 1966.

15. J. A. DiCarlo, "Anelastic Deformation of Boron Fibers," Scripta Met. 10 (2) 115-119 (1976).

16. Z. Hashin, "Complex Moduli of Viscoelastic Composites - II. Fiber Reinforced Materials," Int. J. Solids Struct., 6, 797-807 (1970).

17. A. G. Metcalfe and M. J. Klein, pp. 125-168 "Effect of the Interface on Longitudinal Tensile Properties," Composite Materials, Vol. 1, Edited by A. G. Metcalfe, Academic Press, New York, 1974.

18. E. L. Kern, D. W. Hamill, H. W. Deem, and H. D. Sheets, pp. S25-S32 "Thermal Properties of β-Silicon Carbide from 20 to 2000°," Silicon Carbide, Edited by H. K. Henisch, Pergamon, New York, 1969.

19. G. A. Slack, "Thermal Conductivity of Pure and Impure Silicon, Silicon Carbide, and Diamond," J. Appl. Phys., 35 (12) 3460-3466 (1964).

TABLE 1. - ROOM TEMPERATURE FIBER PROPERTIES

Fiber type[a]	Diameter, μm, d	Density, g/cm^3		Young's modulus GN/m^2		
				Dynamic		Quasistatic
		Fiber ρ	Sheath[b] ρ_S	Flexural[c] E_b	Axial[b] E_a	Axial[d] E_a
B(W)	142	2.475 (.001)[e]	2.347 (.001)			
	203	2.410 (.001)	2.347 (.001)	400 (2)	401 (2)	404[f] (8)
(SiC)B(W)	145	2.50 (.01)		410 (6)	410 (6)	406[g] (10)
SiC(W)	103	3.38 (.04)	3.14 (.04)	419 (20)	419 (20)	415[h] (11)
SiC(C)	143	2.98 (.02)	3.08 (.02)	414 (9)	390 (9)	390[b] (11)
Al_2O_3	20	3.90[i]	3.90			362[i] (11)

[a]Fiber type notation: (coating) sheath (core or substrate).

[b]Calculated from core and coating properties. See Table 2 and text.

[c]Measured near 10^3 Hz at strains below 10^{-5}.

[d]Measured in tension with typical strain rates of 3×10^{-5}/sec.

[e]Numbers in parentheses are standard deviations of measurements.

[f]Measured at 77 K and corrected for temperature and anelasticity (6).

[g]R. H. Ericksen with 103 μm diameter fibers (9).

[h]R. L. Crane (10).

[i]DuPont (11).

TABLE 2. - CORE AND COATING PROPERTIES

Phase	Diameter (thickness), μm	Density, g/cm^3	Modulus, GN/m^2
Tungsten boride ($W_2B_5 + WB_4$)	17	11[a]	550[a]
Tungsten	13	19	411
Carbon	37	1.7[b]	41[b]
Silicon carbide	(1.5)	3.1	415

[a]Reference 6.

[b]Reference 12.

TABLE 3. - FLEXURAL AND AXIAL DAMPING COEFFICIENTS

Fiber type	β_S	β_c	β_X	γ_S	γ_c	γ_X
B(W)	0.9997	0.0003	------	0.9804	0.0196	------
(SiC)B(W)	.9185	.0003	0.0812	.9401	.0184	0.0415
SiC(W)	.9998	.0002	------	.9851	.0149	------
SiC(C)	.9995	.0005	------	.9929	.0071	------

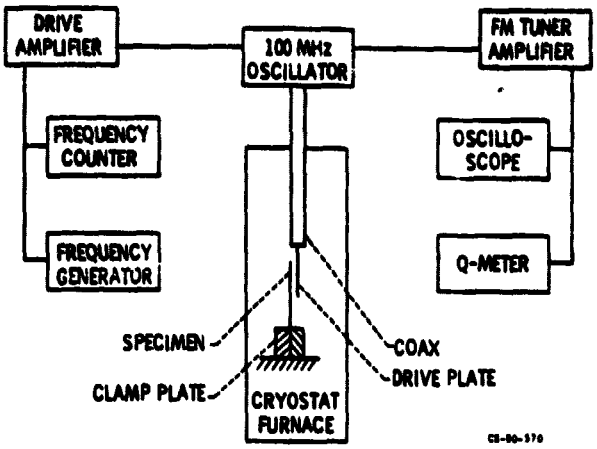

Figure 1. - Schematic diagram of the apparatus and electronics employed for flexural dynamic measurements on single fibers.

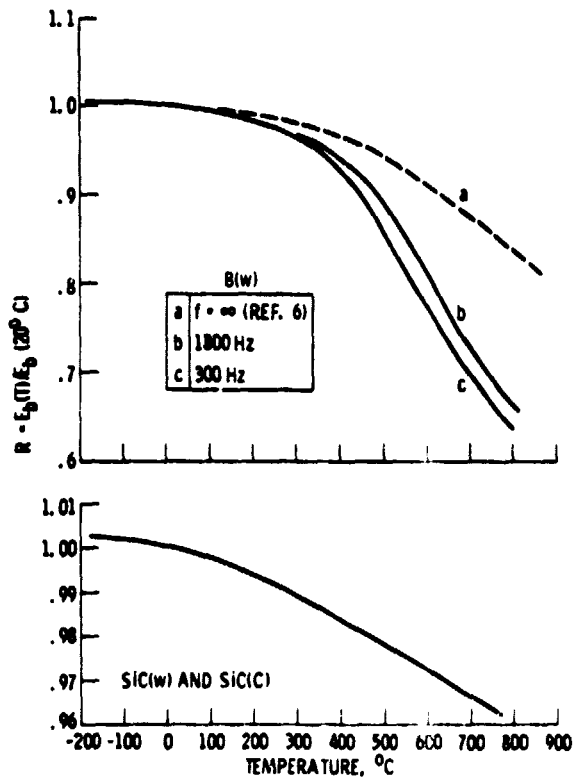

Figure 2. - The normalized dynamic modulus ratio for boron and silicon carbide fibers.

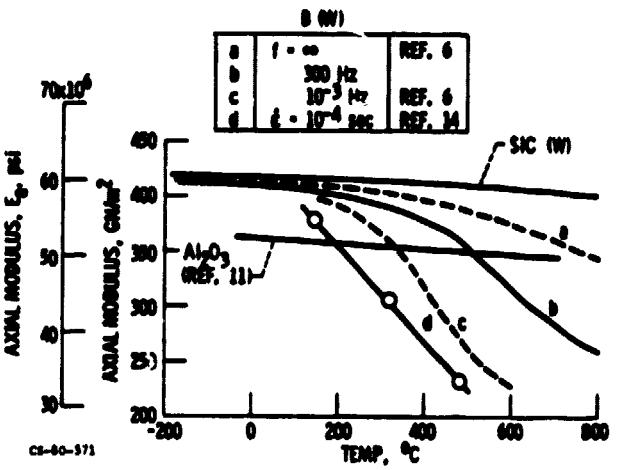

Figure 3. - The axial Young's modulus for boron, silicon carbide, and alumina fibers.

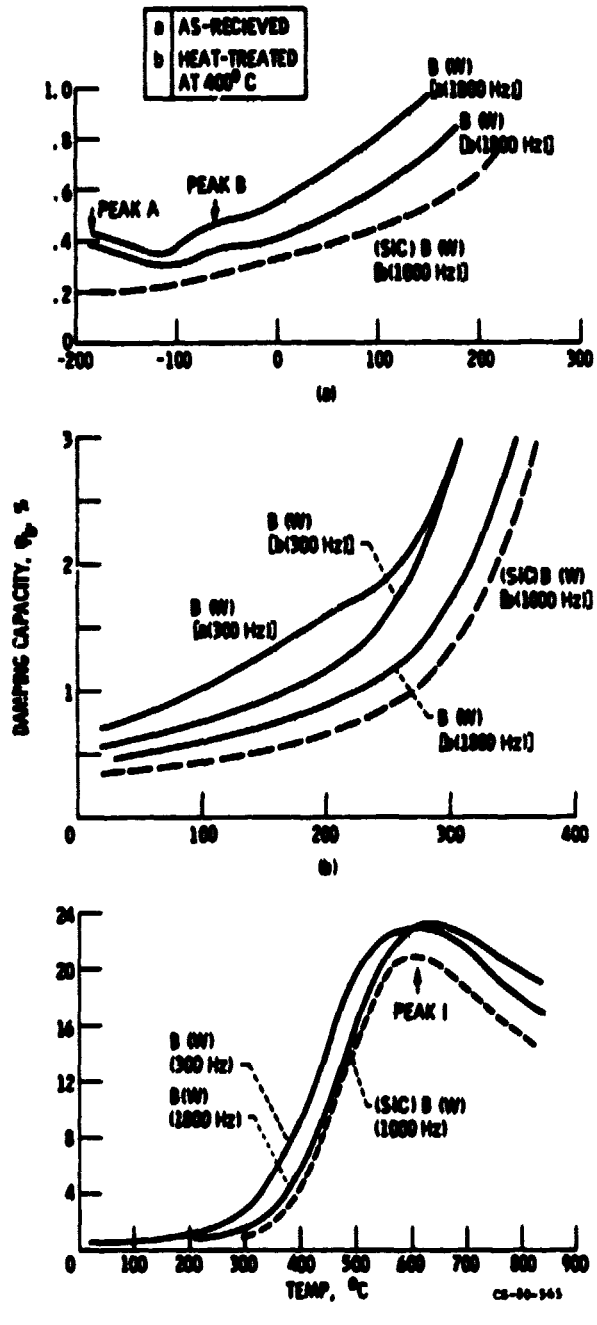

Figure 4. - The damping capacity for boron and silicon carbide-coated boron fibers.

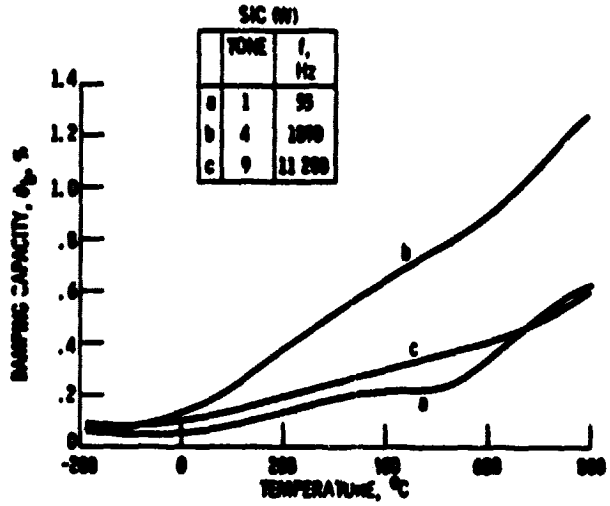

Figure 5. - The damping capacity at three flexural tones of a 109 μm silicon carbide (on tungsten) fiber.

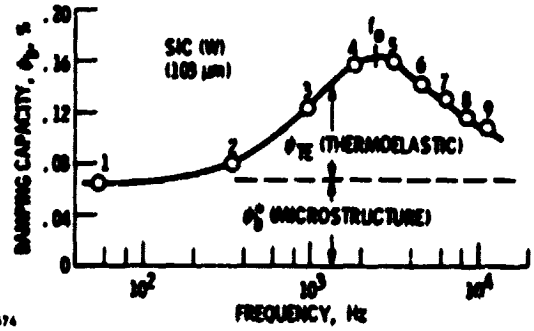

C5-86-574

Figure 6. - Damping capacity at 20° C for the first nine flexural tones of a 109 μm silicon carbide (on tungsten) fiber.

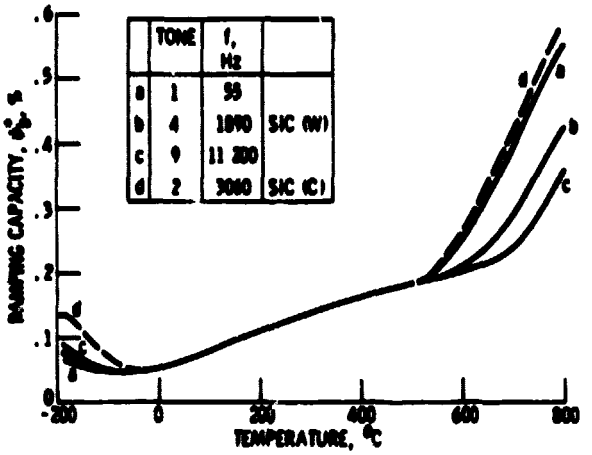

Figure 7. - The microstructural damping capacity for silicon carbide fibers.

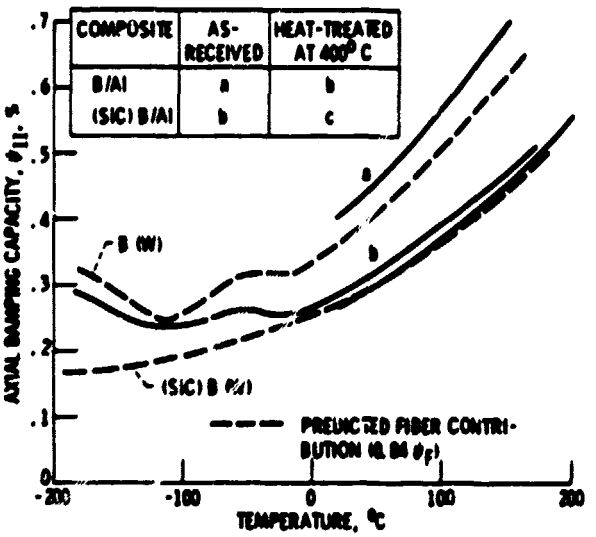

Figure 8. - The axial damping capacity near 2000 Hz for B/Al composites (4). Dashed curves are predicted fiber contributions based on the single fiber damping data of figure 4.

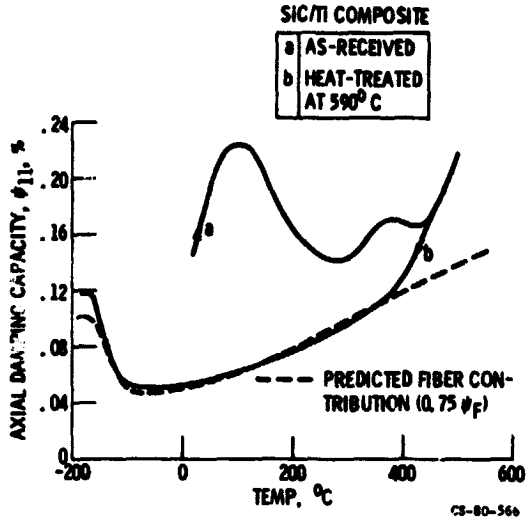

Figure 9. - The axial damping capacity near 2000 Hz for a SiC(C)/Ti composite (4). Dashed curve is predicted fiber contribution based on the single fiber damping data of figure 7.

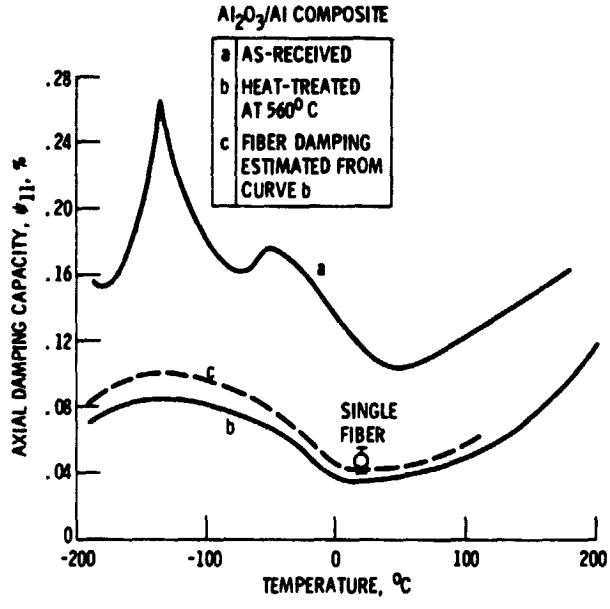

Figure 10. - The axial damping capacity near 2000 Hz for a Al_2O_3/Al composite (4). Dashed curve is alumina fiber damping estimated from curve b. Data point at 20° C was measured on single fiber.

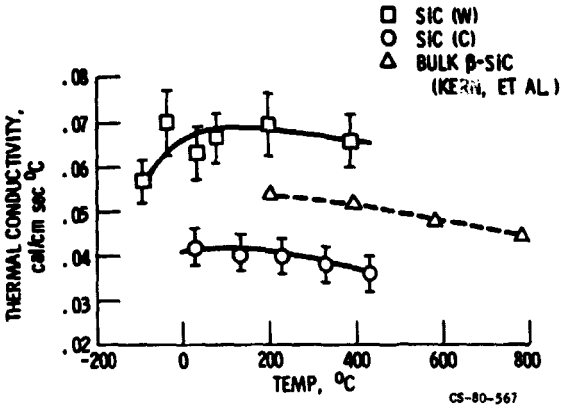

Figure 11. - Transverse thermal conductivity for silicon carbide fibers. Also included are literature data for bulk β-silicon carbide (13).